Bioorganic & Medicinal Chemistry Letters 21 (2011) 7155–7165

Contents lists available at SciVerse ScienceDirect

Bioorganic & Medicinal Chemistry Letters

journal homepage: www.elsevier.com/locate/bmcl

Discovery of a novel class of non-ATP site DFG-out state p38 inhibitors utilizing computationally assisted virtual fragment-based drug design (vFBDD) ☆

Kristofer Moffett *, Zenon Konteatis, Duyan Nguyen, Rupa Shetty, Jennifer Ludington, Ted Fujimoto, Kyoung-Jin Lee, Xiaomei Chai, Haridasan Namboodiri, Michael Karpusas, Bruce Dorsey, Frank Guarnieri, Marina Bukhtiyarova, Eric Springman, Enrique Michelotti

Ansaris, Four Valley Square, 512 East Township Line Road, Blue Bell, PA 19422, USA

ARTICLE INFO

Article history:
Received 8 August 2011
Revised 15 September 2011
Accepted 19 September 2011
Available online 28 September 2011

Keywords:
p38 Kinase
Virtual fragment-based drug design
DFG-out conformation

ABSTRACT

Discovery of a new class of DFG-out p38α kinase inhibitors with no hinge interaction is described. A computationally assisted, virtual fragment-based drug design (vFBDD) platform was utilized to identify novel non-aromatic fragments which make productive hydrogen bond interactions with Arg 70 on the αC-helix. Molecules incorporating these fragments were found to be potent inhibitors of p38 kinase. X-ray co-crystal structures confirmed the predicted binding modes. A lead compound was identified as a potent (p38α IC_{50} = 22 nM) and highly selective (≥150-fold against 150 kinase panel) DFG-out p38 kinase inhibitor.

Over-expression of pro-inflammatory cytokines such as tumor necrosis factor-α (TNF-α), interleukin-1β (IL-1β), and interleukin-6 (IL-6) have been associated with inflammatory diseases such as rheumatoid arthritis (RA), inflammatory pain and chronic obstructive pulmonary disease (COPD).[1] Protein therapeutics etanercept, infliximab, and adalimumab, which target these cytokines, are considered to be a standard treatment for RA.[2] However, the limitations of protein therapeutics (such as cost and parenteral administration) have stimulated significant research aimed at developing orally bioavailable, small molecule inhibitors of cytokines.

The mitogen activated protein kinase (MAPK) p38 plays a central role in the regulation of the cytokines TNF-α and IL-1β.[3] Studies on expression and activation of p38 isoforms in synovial tissue extracted from RA patients implicated p38α as a potentially relevant target for therapeutic intervention.[4–6] This prompted many research groups to focus on discovering and developing small molecule p38α inhibitors as promising anti-inflammatory drugs.[7,8] While recent clinical data indicate that p38 inhibition alone may not be sufficient for effective treatment of RA,[9,10] several p38 inhibitors have either demonstrated analgesic efficacy in acute post-surgical dental pain in a Phase II clinical trial[11] or are currently being evaluated in the clinic for efficacy in acute inflammatory pain, myelodysplastic syndromes, neuropathic pain, COPD, RA, cardiovascular disease and depression.[10]

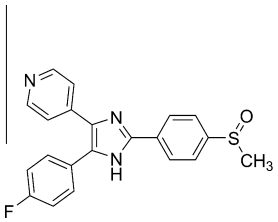

SB203580
1

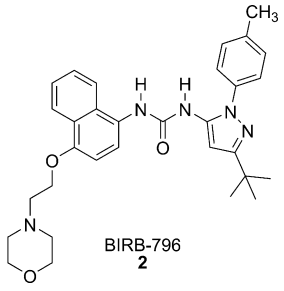

BIRB-796
2

For the treatment of chronic diseases, like RA, kinase inhibitors must be very selective to avoid unwanted side effects that can be caused by off-target kinase inhibition.[7] While selective p38 kinase inhibitors have recently been reported,[12] the early type I and type II p38 inhibitors, such as SB203580 (**1**)[13] and BIRB-796 (**2**)[14] were also active against other kinases. It was suggested that this lack of selectivity may have contributed to the failure to progress these compounds in the clinic. These early inhibitors share the key feature of occupying a significant portion of the ATP binding site, making one or more key hydrogen bonds within the highly conserved hinge region.

Abbreviations: TNF-α, tumor necrosis factor alpha; IL, interleuken; RA, rheumatoid arthritis; MAPK, mitogen activated protein kinase; ATP, adenosine triphosphate; COPD, chronic obstructive pulmonary disease; FBDD, fragment-based drug design; LPS, lipopolysaccharide; PBMC, peripheral blood mononuclear cells; FFP, fresh-frozen plasma; GCMC, grand canonical Monte Carlo.

☆ PDB codes for compounds in the text co-crystallized with p38α are as follows: **13a**, 3P5K; **13b**, 3P78; **17a**, 3P7B; **27**, 3P7C; **34a**, 3P7A; **37b**, 3P79.

* Corresponding author.
E-mail address: kmistry@earthlink.net (K. Moffett).

0960-894X/$ - see front matter © 2011 Elsevier Ltd. All rights reserved.
doi:10.1016/j.bmcl.2011.09.078

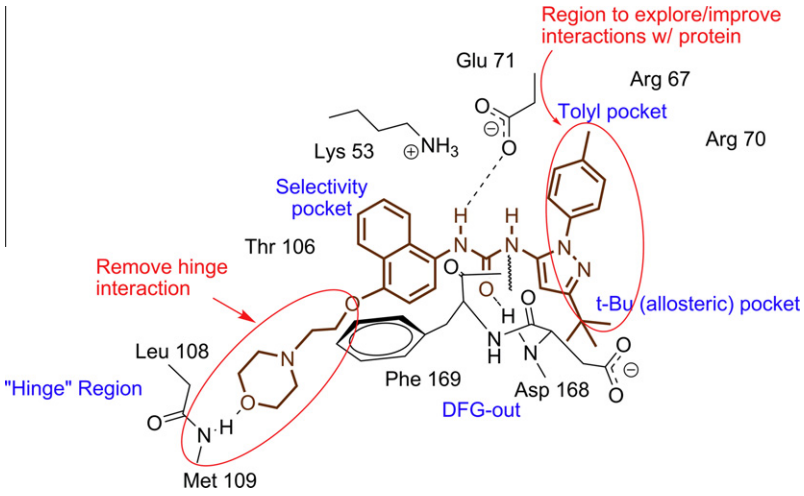

Figure 1. Cartoon of **2** in the p38 DFG-out conformation outlining the various regions (in blue) and important residues. The design strategy involved removing interactions with the hinge, finding replacement fragments for the tolyl pocket, and maintaining interactions with Glu 71, Asp 168, and the selectivity pocket.

Table 1
The *B*-values of selected fragments found in the DFG-out conformation tolyl pocket of p38 kinase

Entry	Fragment	*B*-value
1	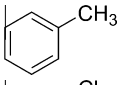	−8.7
2	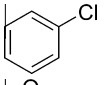	−11.9
3	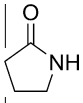	−11.6
4	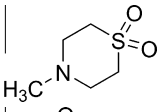	−10.7
5	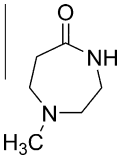	−12.6
6	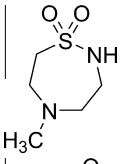	−15.9
7	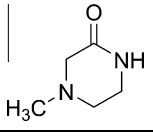	−15.2

We describe here our efforts to discover highly selective, orally bioavailable p38 kinase inhibitors. Our reasoning was that targeting the less conserved, inactive DFG-out conformation of the kinase[15] while avoiding the conserved hinge region would give a better chance at developing selective inhibitors. Recently, two groups reported success with similar strategies.[16] In the original work leading to the development of **2**, compounds having no hinge interaction were reported to be potent against p38 kinase; however, it was thought necessary to add hinge binding elements to improve, at least in part, the physio-chemical properties of the

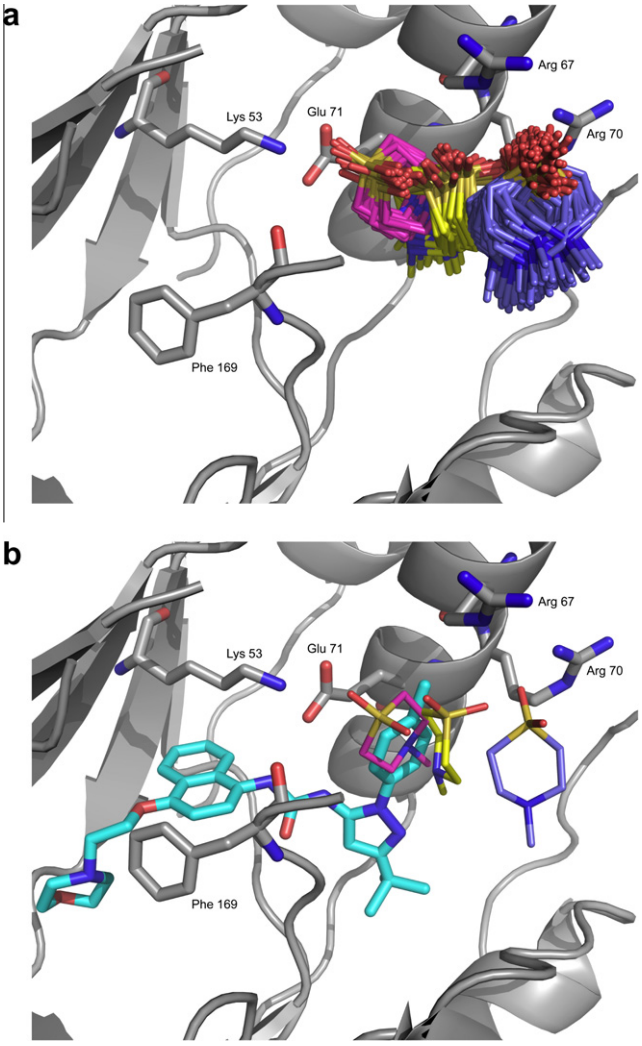

Figure 2. Computationally predicted binding modes of 1,1-dioxothiomorpholine in the DFG-out conformation of p38: (a) output from the calculations gives three clusters of poses for the dioxothiomorpholine mimicking the molecular dynamics of the fragment, in three distinct modes. Mode 1 (pink/gray) interacts with Lys 53. Mode 2 (yellow/dark gray) interacts with Arg 70 with one H-bond. Mode 3 (purple/light gray) interacts with Arg 67 or both Arg 67 and Arg 70; (b) compound **2** (light blue/white) is overlaid with one representative pose from each cluster shown in Fig. 2a, and shows the overlap of the tolyl moiety with binding mode 1.

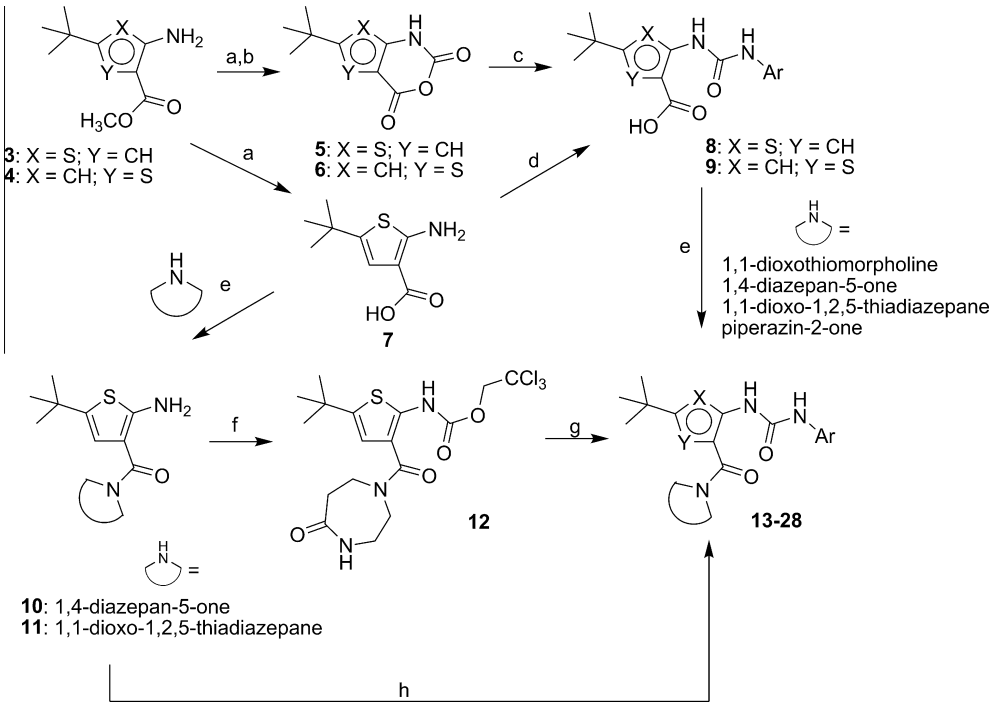

Scheme 1. Synthesis of compounds containing thiophene core. Reagents and conditions: (a) KOH, 1:1 MeOH:H_2O, 80 °C, >95%; (b) 2 M phosgene in toluene, H_2O, r.t. >90%; (c) $ArNH_2$, THF, 70 °C, 75–95%; (d) ArNCO, THF, 35–95%; (e) cyclic amine, EDCI, HOBt, DCM and/or DMF, 39–100%; (f) TrocCl, NaOH, 1:2 H_2O:EtOAc, 5–15 °C, 17–76%; (g) aniline, DMSO, DIEA, 80 °C, 18 h, 13–60%; (h) ArNCO, toluene or THF, 80 °C, 18 h, 10–58%.

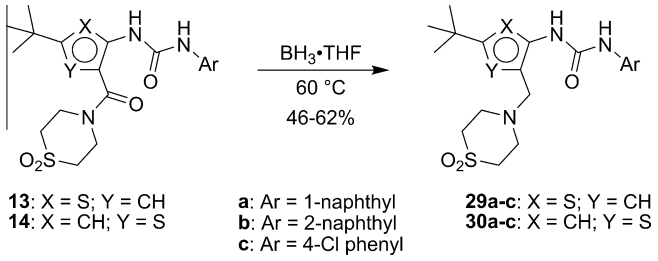

Scheme 2. Reduction of amide to give compounds with a methylene linker.

compounds.[14,15] The challenge for us was to demonstrate that selective, potent and druggable compounds could be made without significant interaction with the hinge region.

The strategy we used to develop novel p38 kinase inhibitors having no hinge interaction is outlined in Figure 1. The urea interactions with Glu 71 and the backbone NH of Asp 168, as well as the *t*-butyl group in the DFG-out pocket were all interactions that would be maintained. Therefore, we focused the computational effort on evaluating fragments in the selectivity pocket and the tolyl pocket. In order to maximize the drug-like character, any newly designed compounds needed to reduce the hydrophobicity of compounds containing both naphthyl and tolyl moieties. Finding a fragment that had enough hydrophobic character to interact with the tolyl pocket and polarity or non-aromatic character to increase drug-like properties had high priority.

We have previously described our fragment-based computational design approach,[17,18] which uses a grand canonical Monte Carlo (GCMC) simulation to generate ensembles of small organic

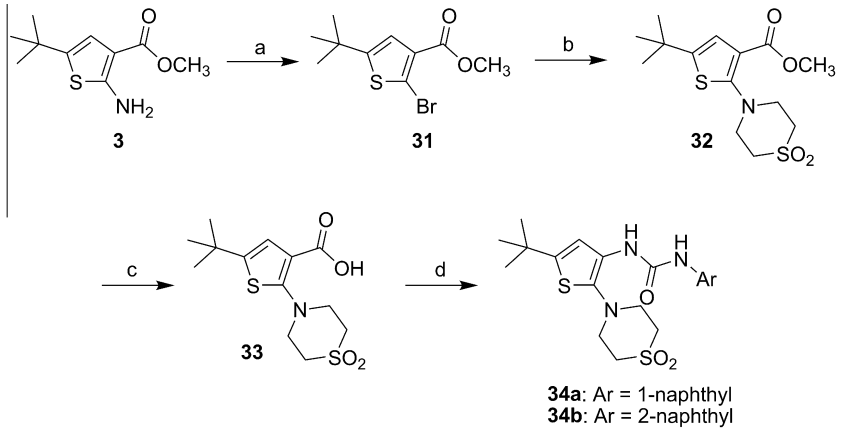

Scheme 3. Synthesis of compound having fragment directly linked to thiophene corre. Reagents and conditions: (a) (i) HCl, $NaNO_2$, H_2O, 0 °C, (ii) $CuBr_2$, 100 °C, 35–60%; (b) dioxothiomorpholine, Cs_2CO_3, $Pd_2(dba)_3$, xantphos, 1,4-dioxane, 85 °C, 18 h, 50%; (c) NaOH, 3:1 MeOH:H_2O, 80 °C, 2 h, quant.; (d) (i) TEA, DPPA, 100 °C, 2 h, (ii) $ArNH_2$, 100 °C, 3 h, 25%.

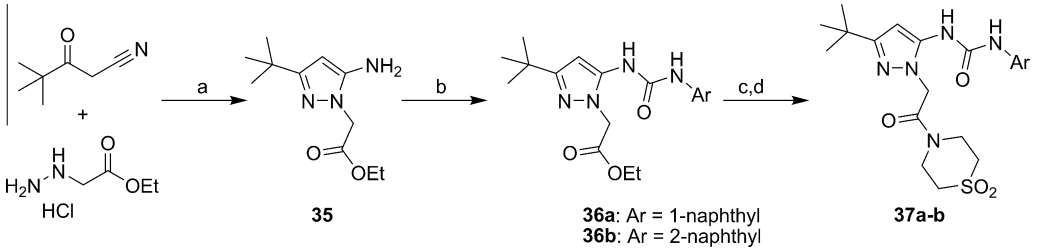

Scheme 4. Synthesis of two-atom linker compounds using pyrazole core. Reagents and conditions: (a) DIEA, toluene, reflux; (b) ArNCO, toluene, reflux, 47–59% (two steps); (c) NaOH, 2:1:1 THF:MeOH:H_2O, r.t.; (d) amine, EDCI, HOBt, DCM, r.t., 22–29% (two steps).

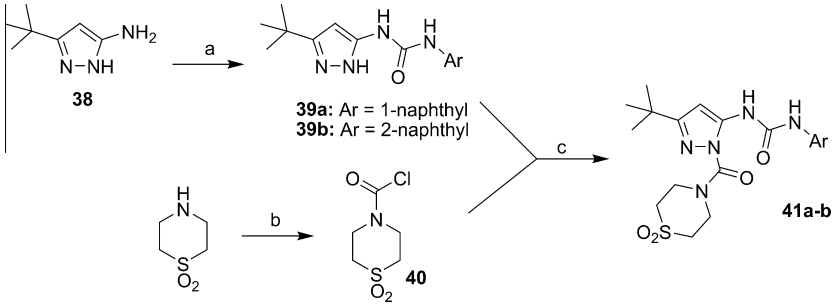

Scheme 5. Synthesis of one-atom linker compounds with pyrazole core. Reagents and conditions: (a) isocyanate, toluene, reflux, 50–58%; (b) phosgene, DIEA, DCM, 0 °C to r.t.; (c) DIEA, 1,4-dioxane, 70 °C, 15–21 h, 17–23%.

Table 2
Evaluation of dioxothiomorpholine fragment, thiomorpholine derivatives and linker strategies against p38 kinase[a]

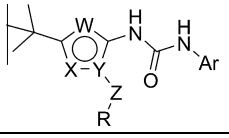

R	W	X	Y	Z	Ar	Compound	p38α IC_{50} (μM)
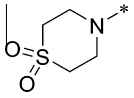	S	CH	C	CO	1-Naphthyl-	**13a**	0.076
	S	CH	C	CO	2-Naphthyl-	**13b**	0.11
	S	CH	C	CO	4-ClPh-	**13c**	0.25
	S	CH	C	CH_2	1-Naphthyl-	**29a**	0.22
	S	CH	C	CH_2	2-Naphthyl-	**29b**	0.9
	S	CH	C	CH_2	4-ClPh-	**29c**	1.7
	CH	S	C	CO	1-Naphthyl-	**14a**	0.13
	CH	S	C	CO	2-Naphthyl-	**14b**	0.12
	CH	S	C	CO	4-ClPh-	**14c**	0.24
	CH	S	C	CH_2	1-Naphthyl-	**30a**	1.2
	CH	S	C	CH_2	2-Naphthyl-	**30b**	5.7
	CH	S	C	CH_2	4-ClPh-	**30c**	16
	CH	S	C	-	1-Naphthyl-	**34a**	0.52
	CH	S	C	-	2-Naphthyl-	**34b**	2
	CH	N	N	CH_2CO	1-Naphthyl-	**37a**	6.4
	CH	N	N	CH_2CO	2-Naphthyl-	**37b**	2.3
	CH	N	N	CO	1-Naphthyl-	**41a**	3.5
	CH	N	N	CO	2-Naphthyl-	**41b**	10
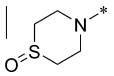	S	CH	C	CO	1-Naphthyl-	**15**	>10
	S	CH	C	CO	1-Naphthyl-	**16**	2.0

[a] The p38 kinase IC_{50} values were determined by measuring the incorporation of ^{33}P from γ-[^{33}P] ATP into the GST-ATF-2 protein substrate as described in the Experimental (see Supplementary data). IC_{50} Values were calculated by non-linear regression with sigmoidal dose-response equation in GraphPad Prism® using data generated in two independent dose response experiments.

fragments, calculate the free energy of binding of these fragments to a protein, and assemble these fragments into potential drugs. These ensembles, or clusters of poses, for each fragment and for each molecule built by the GCMC method represents the dynamic molecular motion of the ligand instead of a single static pose. We applied this virtual fragment-based drug design (vFBDD) approach

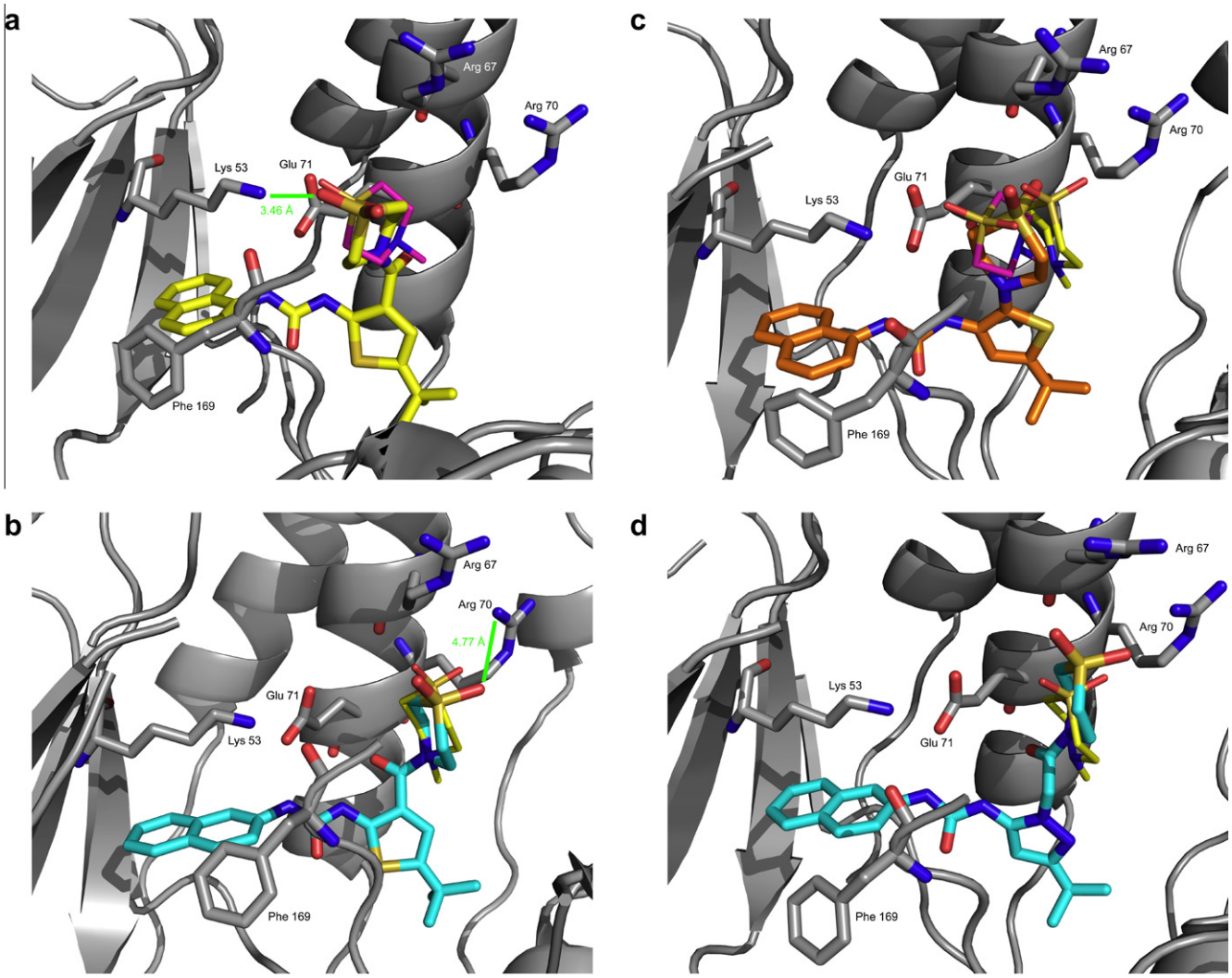

Figure 3. X-ray co-crystal structures of DFG-out compounds in p38α with overlays of representative poses from the predicted binding modes 1 and/or 2 of the dioxothiomorpholine fragment (distances shown are measured from atom centers): (a) compound **13a** (yellow/white) showing overlap with a representative pose from predicted binding mode 1 (pink/dark gray); (b) compound **13b** (light blue/white) showing overlap with a representative pose from binding mode 2 (yellow/dark gray). Comparison to Fig. 3a shows how the 2-naphthyl substitution has extended the dioxothiomorpholine out of binding mode 1; (c) compound **34a** (orange/white) showing the dioxothiomorpholine moiety occupying space midway between binding modes 1 (pink/dark gray) and 2 (yellow/gray); (d) compound **37b** (light blue/white) showing the dioxothiomorpholine moiety in a position above binding mode 2 (yellow/dark gray).

to evaluate fragments and their preferred interactions with the p38 protein.

The interactions of eight hundred fragments with the 1kv2 structure of p38 kinase were simulated, and computed free energies were obtained.[19] Fragments containing sp^3 hybridized nitrogens were simulated in the non-protonated state. For each fragment, a distribution or cluster of poses of equivalent energy was found at various sites of interest on the protein surface. The energy values for each cluster were given as a *B*-value, which is a dimensionless number directly related to the free energy of binding.[17] In the selectivity pocket, multiple fragments (mostly aromatic) were found with favorable energies. Some of these fragments were selected to be used in new compounds as naphthalene replacements. A variety of fragments showed up in the tolyl pocket including aromatic, aliphatic, polar and mixed character fragments.

From these results, the tolyl pocket fragments went through an evaluation process. Fragments with unfavorable *B*-values were discarded, leaving about fifty having favorable *B*-values compared to the tolyl fragment. Fragments with *B*-values within ~10 units were

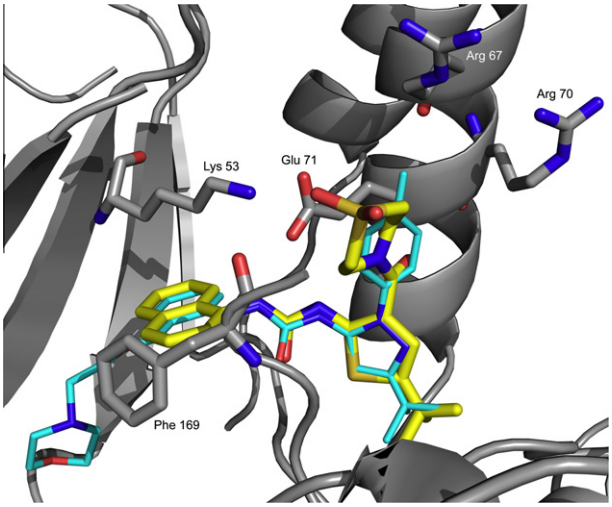

Figure 4. X-ray co-crystal structure of **13a** (yellow/white) with overlay of **2** (light blue/dark grey) showing the two ring methylenes in the hydrophobic tolyl pocket.

Table 3
Evaluation of dioxothiomorpholine replacements[a]

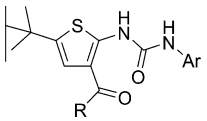

R, Ar		Assay (IC_{50} and EC_{50} values in μM)	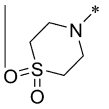 **13**	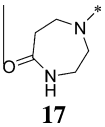 **17**	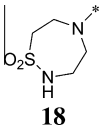 **18**	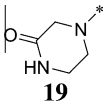 **19**
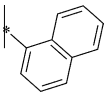	**a**	p38α: PBMC:	0.076 2.5	0.018 2.5	0.11 1.3	0.025 >3
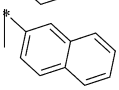	**b**	p38α: PBMC:	0.11 2.7	0.012 2.8	0.018 2.5	0.012 0.27
	**c**	p38α: PBMC:	0.25 2.1	0.03 0.59	0.083 1.6	0.086 2.8

[a] The p38 kinase IC_{50} values were determined by measuring the incorporation of ^{33}P from γ-[^{33}P] ATP into the GST-ATF-2 protein substrate. Cellular assay PBMC IC_{50} values were determined by measuring LPS-induced TNF-α production in peripheral blood monocyte cells (PBMC) as described in the Experimental (see Supplementary data). IC_{50} values were calculated by non-linear regression with sigmoidal dose-response equation in GraphPad Prism® using data generated in two independent dose response experiments.

considered similar. Table 1 shows a subset of these fragments. Entries 1–4 were included in the initial round of selection while entries 5–7 were evaluated in a second iterative round after data on the first compounds were collected.

Further selections were made based on the criteria we had set: (1) preferably non-aromatic; (2) some hydrophobic character; (3) polar functionality; (4) improved drug-like properties. Aromatic fragments, such as chlorobenzene (entry 2, Table 1), were discarded as we wanted to reduce some of the aromatic character in any new compounds. Fragments having polarity, such as carbonyl or sulfoxide, and hydrophobocity, such as the ring methylenes seen in structures like entries 3–7 in Table 1 met our criteria. While the polarity and saturated ring systems would reduce aromaticity and improve drug-like properties, enough hydrophobicity would remain in the methylenes to interact with the hydrophobic nature of the tolyl pocket.

An evaluation based on synthetic feasibility was used to select the final fragments. In order to quickly gather data from an initial set of compounds, we wanted fragments that could easily be incorporated into compounds with core structures already validated to have activity towards p38 kinase. These core structures would include 5-membered ring heterocycles similar to what is found in compound **2**. For this reason we felt that compounds such as pyrrolidonone (entry 3, Table 1) would not be suitable since the chemistry required to attach it to the core systems we had in mind would be more elaborate and time consuming. Fragments with hetero-atoms in appropriate positions, like those seen in entries 4–7 in Table 1, could more easily be incorporated into proof-of-concept compounds.

The first fragment identified from the simulation and selection process was 1,1-dioxothiomorpholine (entry 4, Table 1). The computational simulation output shows the fragment as a cluster of poses in various regions of the protein. Each cluster is identified as a potential binding mode for that fragment to the protein (Fig. 2). Three binding modes for this fragment were found (Fig. 2a): the first is dominated by an H-bond interaction with Lys 53 (mode 1); the second has a single H-bond interaction with Arg 70 (mode 2); the third has two H-bond interactions with Arg 67 or with both Arg 67 and Arg 70 (mode 3).

Overlays of the fragment distributions with **2** showed that modes 1 and 2 could be accessed by either a direct bond to a 5-membered ring core or through one or two atom linkers (Fig. 2b). Binding mode 3 may also be linked to a core by a two atom linker but the computationally minimized small molecule structure showed that it would only cover the edge of the dioxothiomorpholine distribution. Such compounds would not be fully representative of the predicted mode and may not be as active as compounds that put the fragment in the center of the predicted distribution.

We chose to utilize both a thiophene urea core and a pyrazole urea core as the scaffolds to assess the fragments suggested by our computational methodology. Both cores have the advantage of having been incorporated into active p38 compounds[15,20] and having the synthetic feasibility to make the targeted compounds. The thiophene core was used to make compounds with the fragment directly bonded and one-atom linked to the core while the pyrazole core was used to prepare compounds with the fragment attached via one- and two-atom linkages.

Starting from the thiophene aminoesters **3** and **4**,[21] the carbonyl-linked target compounds were prepared via four separate routes (Scheme 1). Anilines with sufficient nucleophilicity utilized oxazinedione intermediates **5** and **6** while less reactive anilines were incorporated via an isocyanate using amino acid **7**. Amide formation with the desired amine containing fragments allowed us to rapidly arrive at the target compounds (**13–28**). Some compounds were made via a parallel synthesis methodology utilizing intermediates **10–12**. The methylene linked compounds **29a–c** and **30a–c** were made from the amides **13a–c** and **14a–c** by reduction using borane (Scheme 2). Direct-linked compounds **34a** and **34b** were synthesized via a key palladium mediated coupling (Scheme 3). It should be noted that the conversion of **4** to the bromide (analogous to **31**) was accomplished but all attempts to add dioxothiomorpholine using various conditions failed to give the desired product (analog of **32**).

Using a pyrazole core more easily allowed for synthesis of compounds with a two atom linker to the fragment. Cyclization of 4,4-dimethyl-3-oxopentanenitrile with ethyl 2-hydrazinylacetate hydrochloride (Scheme 4) gave the amino pyrazole core (**35**) which

subsequently allowed for the formation of the desired products **37a–b**.

One atom linked pyrazole compounds were made by first reacting aminopyrazole **38** with 1- or 2-isocyanatonaphthalene in refluxing toluene to give products **39a–b** with the desired regiochemistry (Scheme 5). Coupling pyrazole ureas **39a–b** with dioxothiomorpholine carbamoyl chloride **40** gave the desired products **41a–b**.

Initial evaluation of inhibitors containing the 1,1-dioxothiomorpholine moiety was done using both thiophene and pyrazole cores with naphthalene and 4-chlorobenzene occupying the selectivity pocket. Compounds with a carbonyl linker to either of the thiophene cores (**13a–c** and **14a–c**) showed good potency in a p38 kinase assay with IC_{50} values at or below 250 nM (Table 2). There was no significant difference in activity between the 2- and 3-aminothiophenes. Replacement of the carbonyl with a methylene significantly reduced activity (compare **13a–c** with **29a–c** and **14a–c** with **30a–c**). Compounds with the dioxothiomorpholine directly connected to the core (**34a–b**) also showed decreased potency. The carbonyl linker may have the proper balance between flexibility (compared to directly bonded compounds) and rigidity (compared to the methylene-linked compounds) to provide an optimal conformation. The dioxothiomorpholine oxygens are important for compound binding as demonstrated by the decreased activity for the compound containing thiomorpholine (compare **13a** with **16**). Interestingly, compound **15,** containing the mono-oxythiomorpholine, also had reduced activity. Compounds with a naphthyl moiety had increased activity over the 4-chlorophenyl (compare **13a–b** and **14a–b** with **13c** and **14c**). This could be due to better space filling in the hydrophobic selectivity pocket by the larger naphthalene moiety. The trend is exaggerated when the compounds are less active (see **29a–c** and **30a–c**).

The carbonyl linker on the pyrazole core was about 50-fold less active (compare **13a–b** with **41a–b**). This could be due to either a difference in the electronics of the two classes of molecules affecting their interaction with the protein, a difference in how each core presents the dioxothiomorpholine moiety to the protein, or a combination of the two. Addition of the two atom linker to the pyrazole core showed no enhancement of activity (compare **41a–b** with **37a–b**).

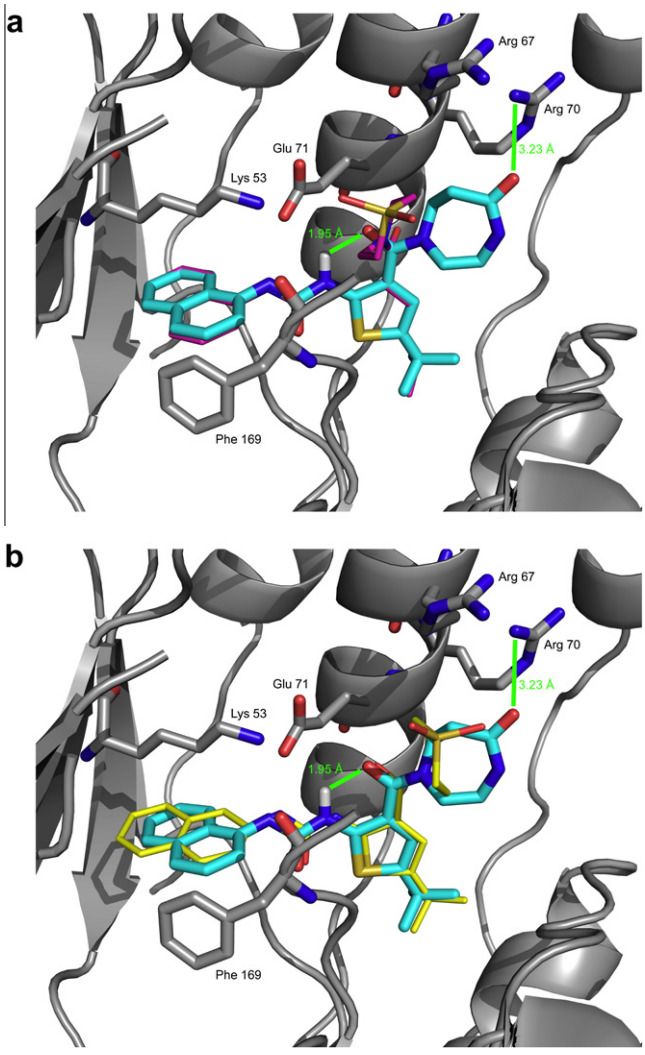

Figure 5. X-ray co-crystal structure of **17a** (light blue/white) in p38 kinase: (a) overlay with the co-crystal structure of **13a** (pink/dark gray); (b) overlay with the co-crystal structure of **13b** (yellow/dark gray). Compound **17a** has the diazepanone is oriented with the carbonyl pointing towards Arg 70. Also shown is the intramolecular hydrogen bond in **17a** and the hydrogen bond between **17a** and Arg 70 (distances are measured from atom centers).

Table 4
Effects of modifications in selectivity pocket with compounds containing diazepanone fragment[a]

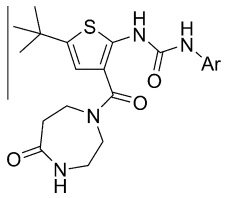

Ar		Assay (IC_{50} and EC_{50} values in μM)	
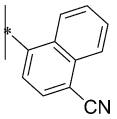	**17d**	p38α: PBMC:	0.006 1.3
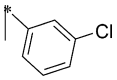	**17e**	p38α: PBMC:	0.042 1.6
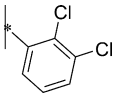	**17f**	p38α: PBMC:	0.01 0.25
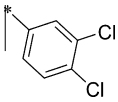	**17g**	p38α: PBMC:	0.013 4.8
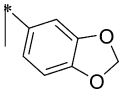	**17h**	p38α: PBMC:	0.022 0.23
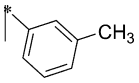	**17i**	p38α: PBMC:	0.08 7
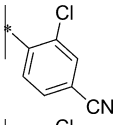	**17j**	p38α: PBMC:	0.13 5.8
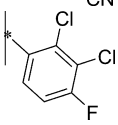	**17k**	p38α: PBMC:	0.002 0.23

[a] The p38 kinase IC_{50} values were determined by measuring the incorporation of ^{33}P from γ-[^{33}P] ATP into the GST-ATF-2 protein substrate. Cellular assay PBMC IC_{50} values were determined by measuring LPS-induced TNF-α production in peripheral blood monocyte cells (PBMC) as described in the Experimental (see Supplementary data). IC_{50} values were calculated by non-linear regression with sigmoidal dose-response equation in GraphPad Prism® using data generated in two independent dose response experiments.

The predicted binding modes for the dioxothiomorpholine fragment were confirmed by solving the X-ray co-crystal structures for compounds containing the various linkers between the core and dioxothiomorpholine (Fig. 3). Compounds with a carbonyl linker were found in two binding modes. Compound **13a**, with the one-atom carbonyl linker, shows the dioxothiomorpholine placed in the binding mode 1 closest to Lys 53 (Fig. 3a) making a hydrogen bond. This is facilitated by the carbonyl being rotated (~90°) away from the plane of the urea. Comparing this to a representative pose from the predicted binding mode 1 shows good overlap between the dioxothiomorpholine moiety and the fragment. The angle of the dioxothiomorpholine moiety in the compound mimics very closely the computationally predicted orientation. Compound **13b**, differing from **13a** by the 2-naphthyl substitution, places the dioxothiomorpholine in binding mode 2 (Fig. 3b). The dioxothiomorpholine moiety again shows good overlap with the predicted binding mode 2. The altered substitution point on the naphthalene helps to push the rest of the molecule closer to Arg 70. The urea NH closest to the ring now has an intramolecular hydrogen bond to the carbonyl linker which is helping to push the dioxothiomorpholine even further out.

Compound **34a**, a direct-connected compound, has the dioxothiomorpholine placed between binding modes 1 and 2 (Fig. 3c). The lower binding affinity of **34a** to p38 kinase compared to **13a** and **13b** would be expected with the dioxothiomorpholine moiety occupying an area between the two predicted higher affinity regions of binding modes 1 and 2. Compound **37b**, the pyrazole having a two atom linker, places the dioxothiomorpholine close to binding mode 2 allowing for a hydrogen bond to Arg 70 (Fig. 3d). However, this linker pushes the moiety slightly up out of the computed optimal distribution closer to the C-helix and side-chain carbons of Arg 67 thus increasing unfavorable interactions with the protein, reflected in the poor activity of **37b**.

Overlaying the structures of **13a** and **2** shows how the naphthyl and core 5-membered ring systems overlap nicely, as would be expected (Fig. 4). Two methylenes from the dioxothiomorpholine ring are positioned to interact with the hydrophobic region occupied by the tolyl moiety of **2**.

Having established an optimal linking strategy, dioxothiomorpholine isosteres were evaluated with the expectation that they would interact with Arg 70 through a hydrogen bond, based on the simulation results. Compounds containing the isosteres showed an improvement in p38 kinase potency of 6–9-fold (diazepanones **17a–c**), 3–6-fold (dioxothiodiazepane **18a–c**) and 3–10 fold (ketopiperazines **19a–c**) compared to the dioxothiomorpholine compounds (Table 3). The cell potency of these compounds, which was assessed by measuring LPS-stimulated TNF-α production in isolated human peripheral blood mononuclear cells (PBMC), remained relatively unchanged, with the exception of **19b** which showed an interesting 10-fold improvement of IC_{50} in the PBMC assay.

The X-ray co-crystal structure of p38 with compound **17a** (Fig. 5) showed the carbonyl linker is in the plane of the urea, making an intramolecular hydrogen bond with the urea NH. This is in

Table 5
Effect of substitution on the diazepanone amide nitrogen[a]

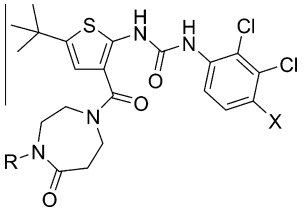

Compound No.	R	X	Assay (IC_{50} and EC_{50} values in μM)		
			p38α	PBMC	FFP–PBMC
20	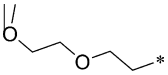	H	0.014	3	–
21	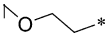	H	0.14	4.2	3.8
22	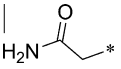	H	0.013	0.83	2.8
23	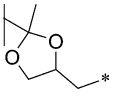	H	0.031	0.39	9.7
24	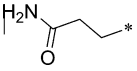	H	0.019	0.16	2.2
25	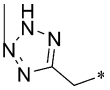	H	0.029	>10	–
26		H	0.039	0.52	6.7
27	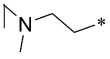	H	0.022	0.39	0.86
28		F	0.073	0.17	1.2

[a] The p38 kinase IC_{50} values were determined by measuring the incorporation of ^{33}P from γ-[^{33}P] ATP into the GST-ATF-2 protein substrate. Cellular assay PBMC and FFP IC_{50} values were determined by measuring LPS-induced TNF-α production in peripheral blood monocyte cells alone (PBMS assay) or in the presence of fresh frozen plasma (FFP–PBMC assay) as described in the Experimental (see Supplementary data). IC_{50} values were calculated by non-linear regression with sigmoidal dose-response equation in GraphPad Prism® using data generated in two independent dose response experiments.

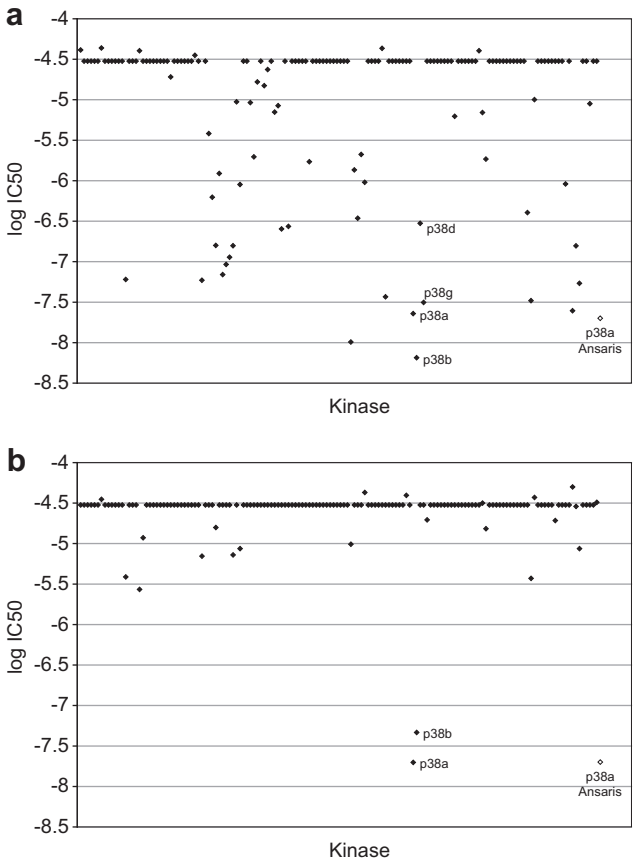

Figure 6. Broad kinase selectivity screening data for compounds **2** and **27** against a panel of 150 kinases using the HotSpot™ filtration binding ^{33}P kinase assay (Reaction Biology, Malvern, PA). In the graph log IC_{50} values (*M*) for kinases in the panel are plotted against an individual kinase in the screen listed in alphabetic order. In-house kinase data for **2** and **27** are plotted for comparison (labeled as 'p38a Ansaris'). The full list of kinases with corresponding IC_{50}s is included in Supplementary data. (a) compound **2** shows activity towards a number of kinases with values comparable to its p38α IC_{50}; (b) compound **27** is >150-fold less potent towards any other kinase compared to p38α (except p38β).

Table 6
Selected data for compound **27**

Hepatocyte (human) $t_{1/2}$	340 min
CaCo2 permiability ($\times 10^{-6}$ cm/s)	P_{ab}: 0.39; P_{ba}: 5.3
Cyp3A4 IC_{50}	0.55 μM
hERG Screen	69% Bound @ 1 μM
Oral PK (rat)	33%F (at 4 mg/kg)

contrast to what was seen with **13a** (Fig. 5a) but is similar to **13b** (Fig. 5b). The carbonyl in the diazepanone ring of **17a** is closer to Arg 70 than the oxygens of the dioxothiomorpholine of **13b**. This allows the carbonyl to form a hydrogen bond with Arg 70. Also, the diazepanone methylenes are in a hydrophobic pocket formed by the side chain carbons of Glu71 and Arg 67. These interactions may account for the improved kinase potency over **13b**.

Compounds containing the diazepanone fragment were further optimized due to their consistently good kinase potency. We evaluated the effect of modifications in the selectivity pocket (Table 4). Replacement fragments were picked, based on results from simulations in the selectivity pocket, to mimic the space filling ability of naphthalene, including phenyl substituted with halogens and polar groups in various configurations. These changes were an attempt to improve cell permeability/activity, which would be reflected in improved PBMC potency. Compounds containing 2,3-dichlorophenyl (**17f**), benzodioxole (**17h**) and 2,3-dichloro-4-fluorophenyl (**17k**) showed 3–10-fold improvement in cell potency while maintaining kinase potency.

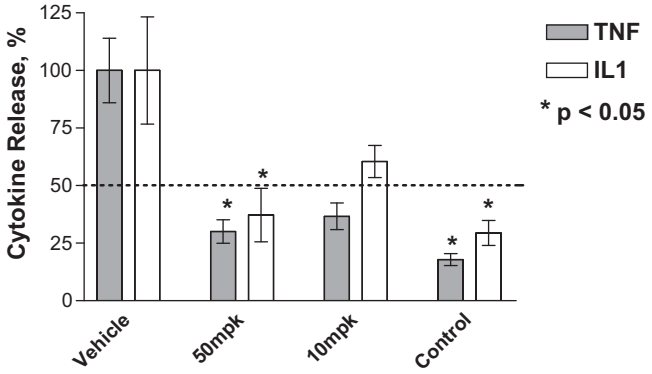

Figure 7. Inhibition of TNF-α and IL-1β for compound **27** in mouse-LPS model. The control is dexamethasone.

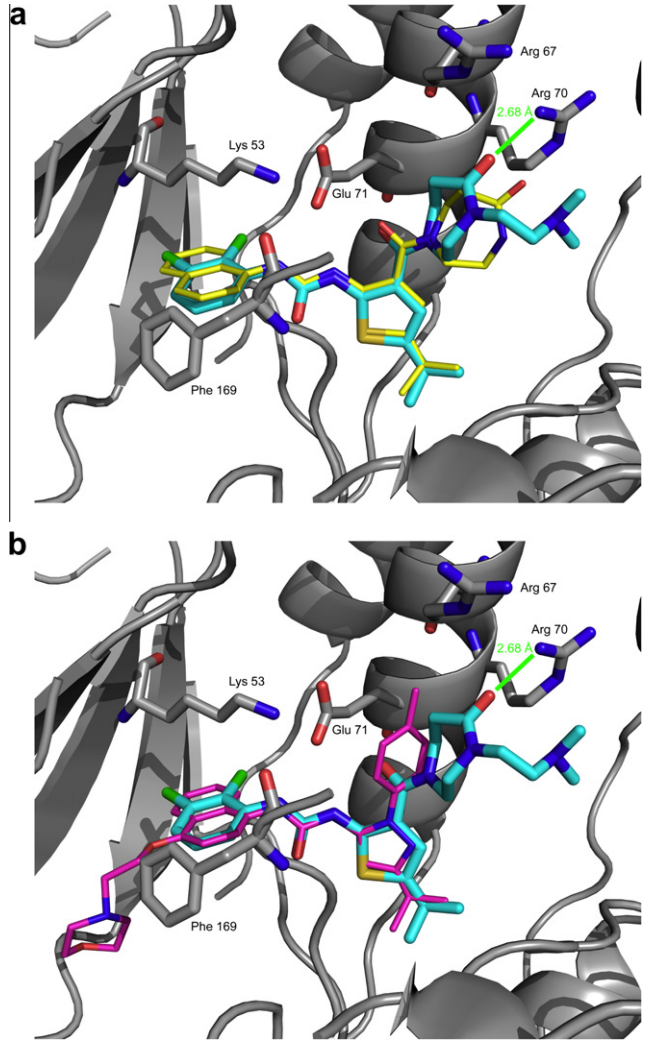

Figure 8. X-ray co-crystal structure of compound **27** (light blue/white) in p38 kinase. (a) overlay of **17a** (yellow/dark gray); (b) overlay of **2** (pink/dark gray) Placement of the dimethylaminoethyl moiety in **27** is an approximation as no electron density beyond the first methylene was seen. H-bond distance is measured from atom centers.

We chose to optimize around **17f** in order to further improve cell potency and pharmacokinetic properties. The co-crystal structure of **17a** showed that the NH of the diazepanone is oriented toward an open region of the protein and therefore could be functionalized to modify compound properties including solubility. Most of the functionality incorporated at this position had good potency towards p38 kinase, similar to **17f**, in the enzymatic assay (Table 5). Most compounds showed sub-micromolar activity in the PBMC assay. However, many compounds lost potency when tested in a cell assay conducted in the presence of human plasma (FFP–PBMC assay). Encouragingly, compound **27** had FFP–PBMC IC_{50} of 860 nM. Interestingly, when the dimethylaminoethyl group was added to **17k** (a compound with better kinase and comparable PBMC activity to **17f**) the resulting compound **28** was found to be 3-fold less potent toward the kinase compared to **27** even though cell potency was comparable.

Compounds **2** (dual DFG-out/ATP site binder) and **27** (non-hinge binder) were evaluated for broad kinase selectivity against a panel of 150 kinases (Fig. 6).[22] Both compounds showed similar activity toward p38α in this assay (**2**: IC_{50} = 0.023 μM; **27**: IC_{50} = 0.020 μM). These data compare well with data obtained from the in-house p38α kinase assay (**2**: IC_{50} = 0.02 μM; **27**: IC_{50} = 0.022 μM). The only other kinase that was inhibited by compound **27** within 150-fold range of p38α IC_{50} was another isoform of p38 kinase – p38β (IC_{50} = 0.05 μM; Fig. 6b). In sharp contrast, compound **2** inhibited 29 kinases out of 150 with IC_{50} values $\leqslant$3.0 μM including 12 kinases being inhibited with IC_{50} values $\leqslant$0.1 μM (Fig. 6a).

Compound **27** was evaluated in various in vitro, in vivo and efficacy studies (Table 6). It showed good stability in human hepatocytes (340 min) and good oral bioavailability in rat (33%F at 4 mg/Kg). Compound **27** also showed the potential for efflux in the CaCo2 assay, sub-micromolar activity towards Cyp3A4 and high binding in the hERG screen. When administered orally in an LPS-challenged mouse model, compound **27** showed a dose-dependant inhibitory effect towards TNF-α and IL-1β release (Fig. 7).

The co-crystal structure of **27** with p38 shows many similarities to the co-crystal of **17a** (Fig. 8a). The dichlorophenyl moiety of **27** occupies similar space in the selectivity pocket as the naphthyl group of **17a**. The hydrogen bond between the carbonyl on the diazepanone with Arg 70 is maintained, and is closer by 0.55 Å compared to **17a**. Electron density for the dimethylaminoethyl moiety beyond the first methylene was not seen in the co-crystal structure. This would indicate that the dimethylaminoethyl moiety did not have any direct interactions with the protein but it does appear to influence the conformation of the diazepanone ring, relative to the unsubstituted ring, without significantly impacting kinase potency. Therefore it appears to act as a solubilizing group, with the effect of enhancing the overall properties of the molecule. A comparison of **27** and **2** (Fig. 8b) shows significant overlapping of the core 5-membered rings, the *t*-butyl and selectivity pockets. Because of the interaction with Arg 70, the diazepanone of **27** only has hydrophobic contacts with the protein along one side of the ring whereas the tolyl moiety of **2** presents an entire face to this hydrophobic region.

We used computational/virtual fragment-based drug design software and methods to design a novel p38 kinase inhibitor with outstanding selectivity. Using this approach we discovered a number of fragments containing both aliphatic and polar functionalities that occupied the tolyl pocket of the DFG-out conformation of p38α kinase. The previously unrecognized 1,1-dioxothiomorpholine fragment along with the isosteres diazepanone, dioxothiodiazepane and ketopiperazine were identified and incorporated into compounds that showed good potency for p38 kinase without needing the interaction with the hinge region. Predicted binding modes of the fragments were confirmed by solving X-ray co-crystal structures. Compounds containing the diazepanone fragment, which make a hydrogen bond to Arg 70 and have hydrophobic interactions in the tolyl pocket, result in excellent selectivity while maintaining potency. Compound **27** demonstrates low nanomolar potency in p38 kinase assay (IC_{50} = 0.022 μM), good cell potency (PBMC EC_{50} = 0.34 μM; FFP–PBMC EC_{50} = 0.86 μM) and high selectivity (>150-fold) in a 150 kinase panel. Compound **27** showed oral bioavailability and demonstrated suppression of TNF-α and IL-1β in an animal efficacy model.

Acknowledgments

The authors wish to thank Syngene International Pvt. Ltd for synthesis of derivatized diazepanone intermediates, Robert Schiksnis for assistance with NMR studies, Brandon Campbell for performing preparative SFC purification and SFC-MS studies, Tim Allison for uploading crystal structures to the PDB, William Moore, Bin Liu and Martha Kelly for scientific contributions and Janet Gaboury valuable help in preparing this manuscript.

Supplementary data

Supplementary data (data table containing results from the broad kinase screen and experimental details for synthesis of compounds) associated with this article can be found, in the online version, at doi:10.1016/j.bmcl.2011.09.078.

References and notes

1. (a) Choy, E. H. S.; Panayi, G. S. *New Eng. J. Med.* **2001**, *344*, 907; (b) Dinarello, C. A. *Curr. Opin. Immunol.* **1991**, *3*, 941.
2. (a) Jarvis, B.; Faulds, D. *Drugs* **1999**, *57*, 945; (b) Seymour, H. E.; Worsley, A.; Smith, J. M.; Thomas, S. H. L. *Br. J. Clin. Pharmacol.* **2001**, *51*, 201; (c) Rutgeerts, P. J. *Aliment. Pharmacol. Ther.* **1999**, *13*, 9.
3. Westra, J.; Limburg, P. C. *Mini-Rev. Med. Chem.* **2006**, *6*, 867.
4. Hale, K. K.; Trollinger, D.; Rihanek, M.; Mantley, C. L. *J. Immunol.* **1999**, *162*, 4246.
5. Korb, A.; Tohidast-Akrad, M.; Cetin, E.; Axmann, R.; Smolen, J.; Schett, G. *Arthritis Rheum.* **2006**, *54*, 2745.
6. Schett, G.; Tohidast-Akrad, M.; Smolen, J. S.; Schmid, B. J.; Steiner, C. W.; Bitzan, P.; Zenz, P.; Redlich, K.; Xu, Q.; Steiner, G. *Arthritis Rheum.* **2000**, *43*, 2501.
7. Goldstein, D. M.; Gabriel, T. *Curr. Top. Med. Chem.* **2005**, *5*, 1017.
8. Pettus, L. H.; Wurtz, R. P. *Curr. Top. Med. Chem.* **2008**, *8*, 1452.
9. Genovese, M. C. *Arthritis Rheum.* **2009**, *60*, 317.
10. Goldstein, D. M.; Kuglstatter, A.; Lou, Y.; Soth, M. J. *J. Med. Chem.* **2010**, *53*, 2345.
11. Tong, S. E.; Daniels, S. E.; Montano, T.; Chang, S.; Desjardins, P. *Am. Soc. Clin. Pharmcol. Ther.* **2004**, *75*, 1.
12. Fabian, M. A.; Biggs, W. H., III; Treiber, D. K.; Atteridge, C. E.; Azimioara, M. D.; Benedetti, M. G.; Carter, T. A.; Ciceri, P.; Edeen, P. T.; Floyd, M.; Ford, J. M.; Galvin, M.; Gerlach, J. L.; Grotzfeld, R. M.; Herrgard, S.; Insko, D. E.; Insko, M. A.; Lai, A. G.; Lelias, J. M.; Mehta, S. A.; Milanov, Z. V.; Velasco, A. M.; Wodicka, L. M.; Patel, H. K.; Zarrinkar, P. P.; Lockhart, D. J. *Nat. Biotechnol.* **2005**, *23*, 329.
13. Cuenda, A.; Rouse, J.; Doza, Y. N.; Meier, R.; Cohen, P.; Gallagher, T. F.; Young, P. R.; Lee, J. C. *FEBS Lett.* **1995**, *364*, 229.
14. Pargellis, C.; Tong, L.; Churchill, L.; Cirillo, P. F.; Gilmore, T.; Graham, A. G.; Grob, P. M.; Hickey, E. R.; Moss, N.; Pav, S.; Regan, J. *Nat. Struct. Biol.* **2002**, *9*, 268.
15. Regan, J.; Breitfelder, S.; Cirillo, P.; Gilmore, T.; Graham, A. G.; Hickley, E.; Klaus, B.; Madwed, J.; Moriak, M.; Moss, N.; Pargelis, C.; Pav, S.; Proto, A.; Swinamer, A.; Tong, L.; Torcellini, C. *J. Med. Chem.* **2002**, *45*, 2994.
16. (a) Liu, H.; Kuhn, C.; Feru, F.; Jacques, S. L.; Deshmukh, G. D.; Ye, P.; Rennie, G. R.; Johnson, T.; Kazmirski, S.; Low, S.; Coli, R.; Ding, Y.-H.; Cheng, A. C.; Tecle, H.; English, J. M.; Stanton, R.; Wub, J. C. *Bioorg. Med. Chem. Lett.* **2010**, *20*, 4885; (b) Ahn, Y. M.; Clare, M.; Ensinger, C. L.; Hood, M. M.; Lord, J. W.; Lu, W.-P.; Miller, D. F.; Patt, W. C.; Smith, B. D.; Vogeti, L.; Kaufman, M. D.; Petillo, P. A.; Wise, S. C.; Abendroth, J.; Chun, L.; Clark, R.; Feese, M.; Kim, H.; Stewart, L.; Flynn, D. L. *Bioorg. Med. Chem. Lett.* **2010**, *20*, 5793.
17. Clark, M.; Guarnieri, F.; Shkurko, I.; Wiseman, J. *J. Chem. Inf. Model.* **2006**, *46*, 231.
18. Clark, M.; Meshkat, S.; Talbot, G. T.; Carnevali, P.; Wiseman, J. S. *J. Chem. Inf. Model.* **2009**, *49*, 1901.
19. For further details of the methodology as it was applied here, see the Supplementary data for a brief description.

20. (a) Dumas, J.; Hatoum-Mokdad, H.; Sibley, R.; Riedl, B.; Scott, W. J.; Monahan, M. K.; Lowinger, T. B.; Brennan, C.; Natero, R.; Turner, T.; Johnson, J. S.; Schoenleber, R.; Bhargava, A.; Wilhelm, S. M.; Housley, T. J.; Ranges, G. E.; Shrikhande, A. *Bioorg. Med. Chem. Lett.* **2000**, *10*, 2051; (b) Redman, A. M.; Johnson, J. S.; Dally, R.; Swartz, S.; Wild, H.; Paulsen, H.; Caringal, Y.; Gunn, D.; Renick, J.; Osterhout, M.; Kingery-Wood, J.; Smith, R. A.; Lee, W.; Dumas, J.; Wilhelm, S. M.; Housley, T. J.; Bhargava, A.; Ranges, G. E.; Shrikhande, A.; Young, D.; Bombara, M.; Scott, W. J. *Bioorg. Med. Chem. Lett.* **2001**, *11*, 9.
21. Ranges, G.; Scott, W.; Bombara, M.; Rauner, D.; Redman, A.; Smith, R.; Paulsen, H.; Chen, J.; Gunn, D.; Renick, J. *PCT Int. Appl.* WO 98/52558, 1998.
22. A table identifying the kinases tested and the resulting IC_{50} values can be found as Supplementary data.